Kinetics of the OH + HCNO Reaction

Wenhui Feng, Justin P. Meyer, and John F. Hershberger*

Department of Chemistry and Molecular Biology, North Dakota State University, Fargo, North Dakota 58105

Received: December 5, 2005; In Final Form: January 24, 2006

The kinetics of the OH + HCNO reaction was studied. The total rate constant was measured by LIF detection of OH using two different OH precursors, both of which gave identical results. We obtain $k = (2.69 \pm 0.41) \times 10^{-12} \exp[(750.2 \pm 49.8)/T]$ cm^3 molecule^{-1} s^{-1} over the temperature range 298−386 K, with a value of $k = (3.39 \pm 0.3) \times 10^{-11}$ cm^3 molecule^{-1} s^{-1} at 296 K. CO, H_2CO, NO, and HNO products were detected using infrared laser absorption spectroscopy. On the basis of these measurements, we conclude that CO + H_2NO and HNO + HCO are the major product channels, with a minor contribution from H_2CO + NO.

1. Introduction

Fulminic acid, HCNO, has recently been identified as an important intermediate in NO-reburning processes for the reduction of NO_x pollutants from fossil-fuel combustion emissions.[1] HCNO originates primarily from the oxidation of acetylene

$$O + C_2H_2 \rightarrow CO + CH_2 \quad (1a)$$

$$\rightarrow HCCO + H \quad (1b)$$

$$HCCO + NO \rightarrow HCN + CO_2 \quad (2a)$$

$$\rightarrow HCNO + CO \quad (2b)$$

Channel 2b has recently been recognized as the major product channel in reaction 2, with the most recent measurements and calculations converging on a branching ratio of $\varphi_{2a} = 0.22-0.28$.[2−6] As a result, the subsequent chemistry of HCNO is of great interest in the overall NO-reburning mechanism. In particular, the OH + HCNO reaction has been identified as a crucial step[1]

OH + HCNO

$$\rightarrow H_2O + (NCO) \quad \Delta H^0_{298} = -364.0 \text{ kJ/mol} \quad (3a)$$

$$\rightarrow NH_2 + CO_2 \quad \Delta H^0_{298} = -413.4 \text{ kJ/mol} \quad (3b)$$

$$\rightarrow HNO + HCO \quad \Delta H^0_{298} = -67.1 \text{ kJ/mol} \quad (3c)$$

$$\rightarrow HCN + HO_2 \quad \Delta H^0_{298} = -73.0 \text{ kJ/mol} \quad (3d)$$

$$\rightarrow CH_2O + NO \quad \Delta H^0_{298} = -235.8 \text{ kJ/mol} \quad (3e)$$

$$\rightarrow CO + H_2NO \quad \Delta H^0_{298} = -247.6 \text{ kJ/mol} \quad (3f)$$

$$\rightarrow CO + H_2 + NO \quad \Delta H^0_{298} = -230.4 \text{ kJ/mol} \quad (3g)$$

The thermochemical information has been obtained from standard tables[7] as well as other references for the heats of formation of HCNO,[5] NCO,[8] and H_2NO.[9] In their modeling study, Miller et al. used an estimated rate constant of $k_3 = 3.32 \times 10^{-11}$ cm^3 molecule^{-1} s^{-1}, with no temperature dependence.[1] This paper also showed ab initio calculations of the OH + HCNO potential energy surface, predicting pathways to product channels 3a, 3c, 3e, and 3g.[1]

In this study, we report the first experimental measurements of the kinetics of the OH + HCNO reaction. In fact, to the best of our knowledge, this is the first report of any direct experimental kinetic measurements on fulminic acid, although a substantial body of literature exists on the kinetics of the more stable isomer HNCO (isocyanic acid).[10−19]

2. Experimental Section

Total rate constant measurements were measured by laser-induced fluorescence (LIF) detection of OH. An amount of 193 or 248 nm excimer laser light (typically ∼5 mJ/pulse) was used to create OH radicals by one of the following two methods

$$N_2O + h\nu \text{ (193 nm)} \rightarrow O(^1D) + N_2 \quad (4)$$

$$O(^1D) + H_2O \rightarrow OH + OH \quad (5)$$

or

$$H_2O_2 + h\nu \text{ (248 nm)} \rightarrow OH + OH \quad (6)$$

The excimer light was made collinear with 306.966 nm probe light from a frequency-doubled Nd:YAG-pumped dye laser. Both beams entered a 91.4 cm reaction cell. Fluorescence was detected at right angles from the laser beams with a PMT mounted against a side window. Signals were recorded on a gated integrator (with 300 ns delay, 200 ns gate width), digitized, and stored on a computer. Timing between excimer and dye pulses was controlled by a computer-controlled digital delay generator. The pump−probe delay was varied to obtain the OH concentration profiles.

Reaction products were detected by infrared diode laser absorption spectroscopy. Several lead salt diode lasers (Laser Components) operating in the 80−110 K temperature range were used to provide tunable IR probe laser light. The IR beam was collimated by a lens and combined with the UV excimer light by means of a dichroic mirror, and both beams were copropagated through a 1.46 m absorption cell. After the UV light was removed by a second dichroic mirror, the IR beam was then passed into a $^1/_4$ m monochromator and focused onto a 1 mm

* To whom correspondence should be addressed. E-mail: john.hershberger@ndsu.edu.

10.1021/jp058305t CCC: $33.50 © 2006 American Chemical Society
Published on Web 03/15/2006

InSb detector (Cincinnati Electronics, ~1 μs response time). Transient IR absorption signals were recorded on a LeCroy 9310A digital oscilloscope and transferred to a computer for analysis. To account for small probe laser thermal deflection effects, signals were collected with the diode laser slightly detuned off of the absorption lines, and such transients were subtracted from the on-resonant transients. This was a small (5−10%) correction for the major products but a more substantial correction for minor products (NO and H_2CO).

SF_6 and CF_4 (Matheson) were purified by repeated freeze−pump−thaw cycles at 77 K. Traces of CO_2 were removed from SF_6 by the use of an Ascarite trap. NO (Matheson) was purified by repeated freeze−pump−thaw cycles at 153 K to remove NO_2 and N_2O. H_2O_2 (Aldrich, 50% in H_2O) was purified by extensive pumping to remove the more volatile water component. After purification, the H_2O_2 solution was estimated to be ~85% pure.

HCNO was synthesized by vacuum pyrolysis of 3-phenyl-4-oximino-isoxazol-5-(4H)-one as described in the literature.[20−22] The precursor (2.0 g) was sublimed from a 50 mL bulb in a 93−96 °C oil bath and passed through a horizontal quartz tube heated to 450 °C in a tube furnace. The products, which included HCNO, HNCO, H_2O, CO_2, and phenyl cyanide, were collected over a 12 h period at 77 K. H_2O and phenyl cyanide were removed by twice passing the products through a 240 K trap. CO_2 and HNCO were removed by vacuum distillation at 192 K. A substantial effort was necessary to optimize conditions for this synthesis. In particular, the 93−96 °C oil temperature was found ideal to vaporize but not decompose the 3-phenyl-4-oximino-isoxazol-5-(4H)-one during the pyrolysis. The purity of the HCNO samples was characterized by FTIR spectroscopy (especially the comparison of the HCNO absorption at 2196 cm^{-1} with the HNCO absorption at 2267 cm^{-1}) and was typically 90% or better. Because HCNO has poor long-term stability, samples were kept frozen at 77 K except when filling the reaction cell. Fresh samples were synthesized for each day's experiments. In general, HCNO could be allowed to stand at room temperature for ~5 min in our Pyrex absorption cell with minimal decomposition, but significant decomposition over ~5 min was commonly observed if the sample was in contact with stainless steel vacuum lines. As a result, the vacuum system was modified to minimize (but not entirely eliminate) exposure of HCNO to metal.

The following molecules were probed using IR diode laser absorption spectroscopy

CO ($v = 1 \leftarrow v = 0$)	R(14) at 2196.664 cm^{-1}
N_2O (00^01) ← (00^00)	P(23) at 2202.744 cm^{-1}
CO_2 (00^01) ← (00^00)	P(14) at 2337.659 cm^{-1}
HCNO (0100^00^0) ← (0000^00^0)	R(10) at 2203.851 cm^{-1}
HNO (100) ← (000)	P(6) at 2667.785 cm^{-1}
H_2CO (100000) ← (000000)	R(10) at 2758.806 cm^{-1}
NO ($v = 1 \leftarrow v = 0$)	R(10.5) at 1912.072 cm^{-1}

The HITRAN molecular database was used to locate and identify the spectral lines of CO, N_2O, H_2CO, and CO_2 product molecules.[23] Other published spectral data were used to locate and identify HCNO[24] and HNO[25] lines. The spectral lines used are near the peak of the rotational Boltzmann distribution, minimizing sensitivity to small heating effects. For CO_2 product molecule measurements, the IR laser beam path was purged with N_2 to remove atmospheric CO_2.

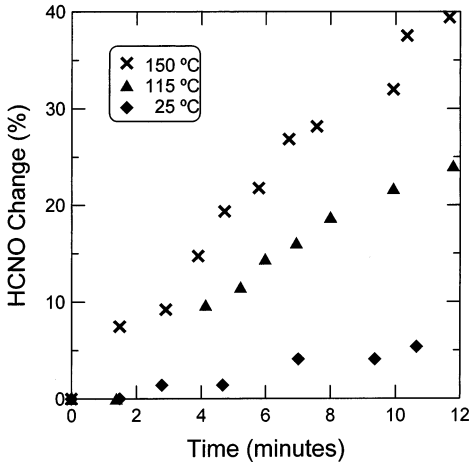

Figure 1. Change in HCNO concentration, monitored by IR absorbance (using the ($0100^{00}0^0$) ← (0000^00^0) R10 line at 2203.851 cm^{-1}) as a function of time in the reaction cell. Temperature: 25 °C (diamonds), 115 °C (triangles), and 150° C (crosses).

Typical experimental conditions were P(HCNO) = 0.20 Torr, $P(H_2O_2)$ = 0.50 Torr, $P(SF_6)$ or $P(CF_4)$ = 1.00 Torr, P(NO) = 0.0−0.50 Torr, and excimer laser pulse energies of ~4 mJ.

3. Results

3.1. Stability of HCNO Samples. A critical aspect of these experiments is the requirement that the HCNO samples be sufficiently stable over the time scale of our experiments. The samples last about a day in a Pyrex bulb at 77 K, but once introduced into the reaction cell, some decomposition or polymerization was inevitable, either due to contact with metal in the vacuum lines or slow reaction with other reagents in the cell. To examine this issue, IR diode laser absorption was used to monitor static HCNO samples as a function of time in the reaction cell. These data are shown in Figure 1. As is apparent, only slight decomposition occurs in room temperature over a 3−5 min period, which is the approximate length of time necessary to collect experimental data. At higher temperatures, decomposition is significantly faster. On the basis of these decomposition curves, we choose 386 K as the maximum temperature to conduct total rate constant experiments. Above 386 K, decomposition occurs sufficiently rapidly enough to significantly compromise the data.

3.2. Total Rate Constants. Figure 2 shows a plot of the OH radical LIF signal as a function of excimer−probe delay time, using N_2O/H_2O (reactions 4 and 5) as the OH radical precursor. In the absence of HCNO reagent, only a very slow decay over the time range 50−300 μs is observed. This decay is attributed to the removal of OH radicals by pathways other than the title reaction, including self-reaction, reaction with other radicals, and diffusion out of the probed region of the reaction cell. Upon the addition of HCNO reagent, a large increase in the OH decay rate is observed. Decay curves such as those shown in Figure 2 were fit to a single exponential over the time range 50−300 μs. Figure 3 shows the resulting decay rates as a function of HCNO pressure. A linear dependence is observed, as is expected if the system obeys pseudo-first-order kinetics (for nonzero P_{HCNO}) and no secondary reactions play a significant role in the OH signals. As per standard kinetic treatment, the slope of this plot is the desired rate constant k_3. The rate constant k_3 obtained in this way was found to be identical within experimental uncertainties for the two OH production methods

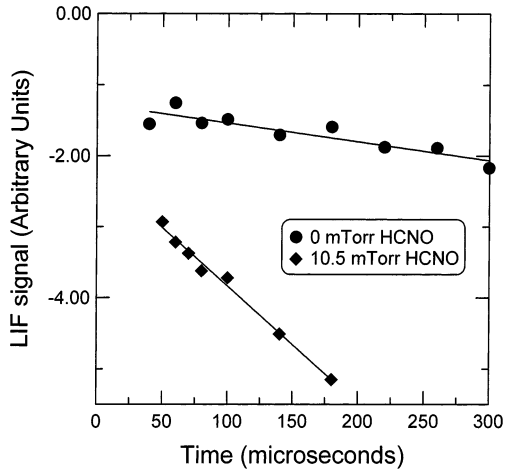

Figure 2. Laser-induced fluorescence signal of OH as a function of photolysis-probe delay time: circles, 0.0 Torr HCNO; diamonds, 0.0105 Torr HCNO. Other conditions: $P(N_2O) = 0.050$ Torr, $P(H_2O) = 0.350$ Torr, $P(SF_6) = 0.50$ Torr, and excimer at 193 nm.

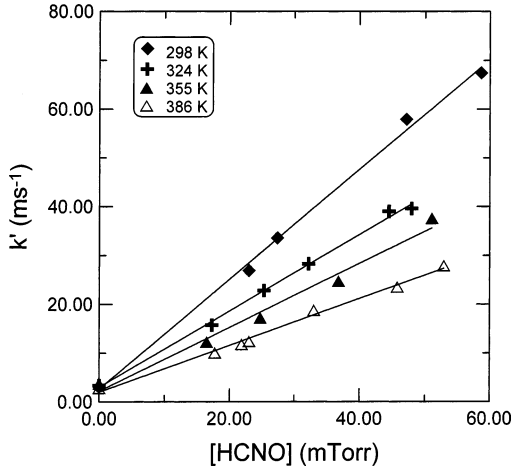

Figure 3. Pseudo-first-order decay rates of the OH radical as a function of HCNO pressure. Conditions: $P(H_2O_2) = 0.50$ Torr, $P(SF_6) = 0.50$ Torr, P(HCNO) = variable, and excimer at 248 nm.

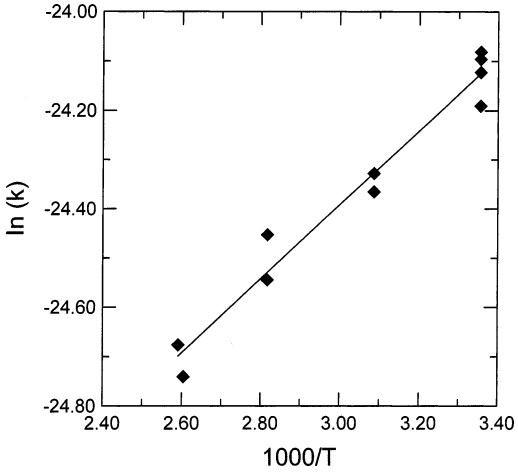

Figure 4. Arrhenius plot for the OH + HCNO reaction.

(reactions 4 + 5 at 193 nm photolysis wavelength vs reaction 6 at 248 nm).

Figure 4 shows an Arrhenius plot for the OH + HCNO reaction. As described above, measurements were limited to a rather narrow temperature range because HCNO decomposition in the reaction cell becomes unacceptably rapid at high temperatures. Nevertheless, the temperature range is sufficient to obtain reasonably precise Arrhenius parameters. We obtain the following rate constants

$$k_3(T) = (2.69 \pm 0.41) \times 10^{-12} \exp[(750.2 \pm 49.8)/T] \text{ cm}^3 \text{ molecule}^{-1} \text{ s}^{-1} \quad (T = 298-386 \text{ K})$$

$$k_3 = (3.39 \pm 0.3) \times 10^{-11} \text{ cm}^3 \text{ molecule}^{-1} \text{ s}^{-1} \text{ at } 296 \text{ K}$$

The error bars in the Arrhenius parameters represent one standard deviation. The error bars in the 296 K value are larger than the standard deviation of 296 K measurements and are based primarily on an estimate of the uncertainty in HCNO concentrations.

The negative activation energy observed in this reaction is typical of radical−radical kinetics and suggests that the reaction proceeds by complex formation, followed by possible rearrangement and decomposition to form products. Direct hydrogen abstraction to form H_2O + CNO (or NCO) would be expected to have a significant positive activation energy and is apparently not a significant contribution in this reaction.

3.3. Product Yields. IR diode laser absorption was used to attempt detection of CO, CO_2, N_2O, NO, CH_2O, and HNO products. Some transient signals are shown in Figure 5. All product yield data were obtained at 296 K.

CO_2 was not successfully detected as a reaction product, primarily because the HCNO samples contained a trace impurity of CO_2 (even a 1% impurity, difficult to remove, affects our measurements). In fact, attempts to detect CO_2 resulted in small negative transients, presumably due to removal or vibrational excitation of CO_2 by the chemistry taking place. We did not investigate this issue at length but simply note that channel 3b is clearly not a major product channel.

The product molecules CO, NO, CH_2O, and HNO were successfully detected upon 248-nm photolysis of a H_2O_2/HCNO/buffer gas mixture. SF_6 buffer gas was used for these experiments, with the exception of CO detection, for which CF_4 buffer gas was used. The choice of buffer gas was motivated by the desire to quickly relax a nascent excited vibrational state distribution to the Boltzmann distribution. Once this relaxation is complete, the absolute concentration of the detected product could be obtained from the population of the probed rotation−vibration state. Previous measurements in our laboratory[6,26−28] as well as vibrational energy transfer measurements[29−32] have demonstrated that SF_6 is an effective buffer gas for the relaxation of vibrationally excited CO_2 and N_2O as well as many other molecules but that CF_4 is a better buffer gas for relaxation of vibrationally excited CO.

N_2O was detected upon 248-nm photolysis of a H_2O_2/HCNO/NO/buffer gas mixture. We attribute N_2O formation to the reaction of NCO with NO

$$\text{NCO} + \text{NO} \rightarrow \text{N}_2\text{O} + \text{CO} \quad (7a)$$

$$\rightarrow \text{N}_2 + \text{CO}_2 \quad (7b)$$

where the branching ratio $\varphi_{7a} = 0.44$ at 296 K.[26] As shown below, however, most or all of the NCO was not produced from reaction 3 but from secondary chemistry.

HCN is not detectable in our diode laser spectrometer because of the lack of available laser diodes in the 3300 cm^{-1} region. As a result, we cannot probe the importance of channel 3d by transient IR spectroscopy. We have, however, obtained static (Fourier transform) FTIR spectra of the reaction mixture with and without precursor after extensive photolysis (1000

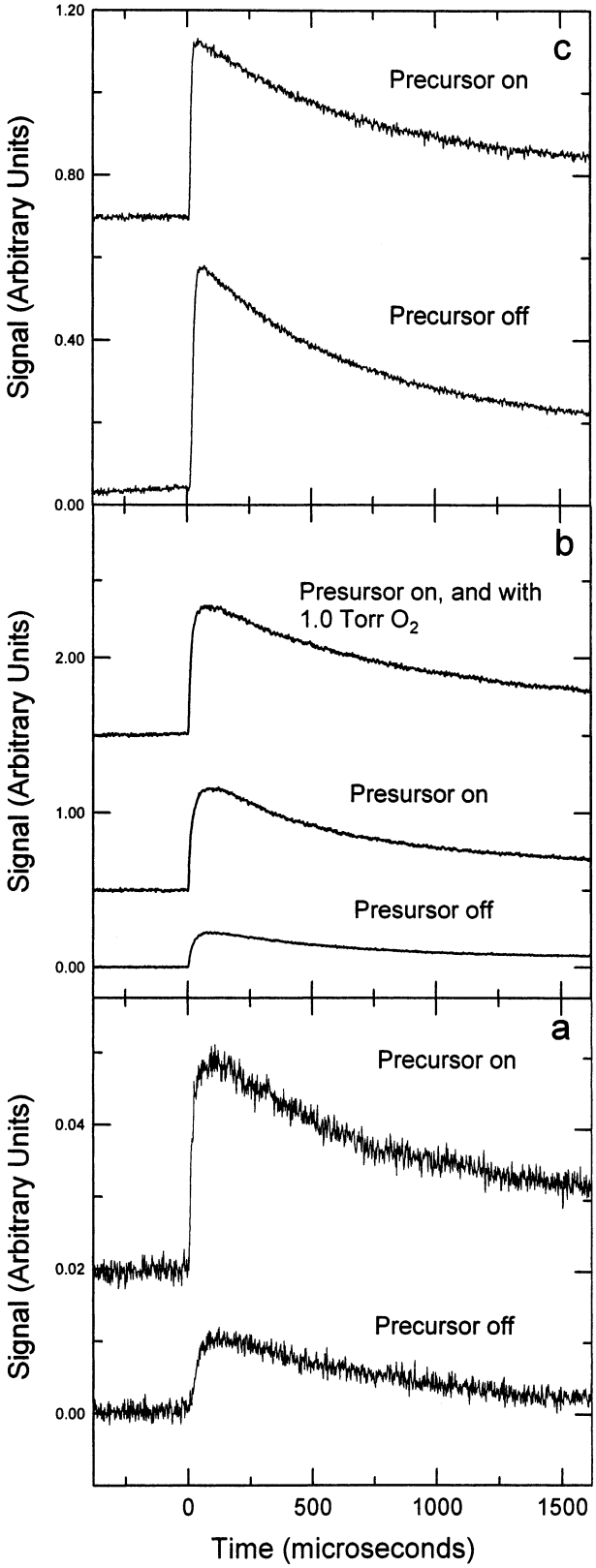

Figure 5. Transient signals of (a) HNO, (b) CO, and (c) N_2O. Reaction conditions: $P(H_2O_2) = 0.50$ Torr (upper traces), $P(H_2O_2) = 0.0$ Torr (lower traces), $P(HCNO) = 0.20$ Torr, $P(SF_6) = 1.00$ Torr (HNO and N_2O transients only), $P(CF_4) = 1.00$ Torr (CO transients only), and $P(NO) = 0.50$ Torr (N_2O transients only).

excimer laser pulses). The stable products observed in the transient experiments are observable in the FTIR, but no HCN attributable to channel 3d (i.e., beyond that produced by HCNO photolysis) was detected.

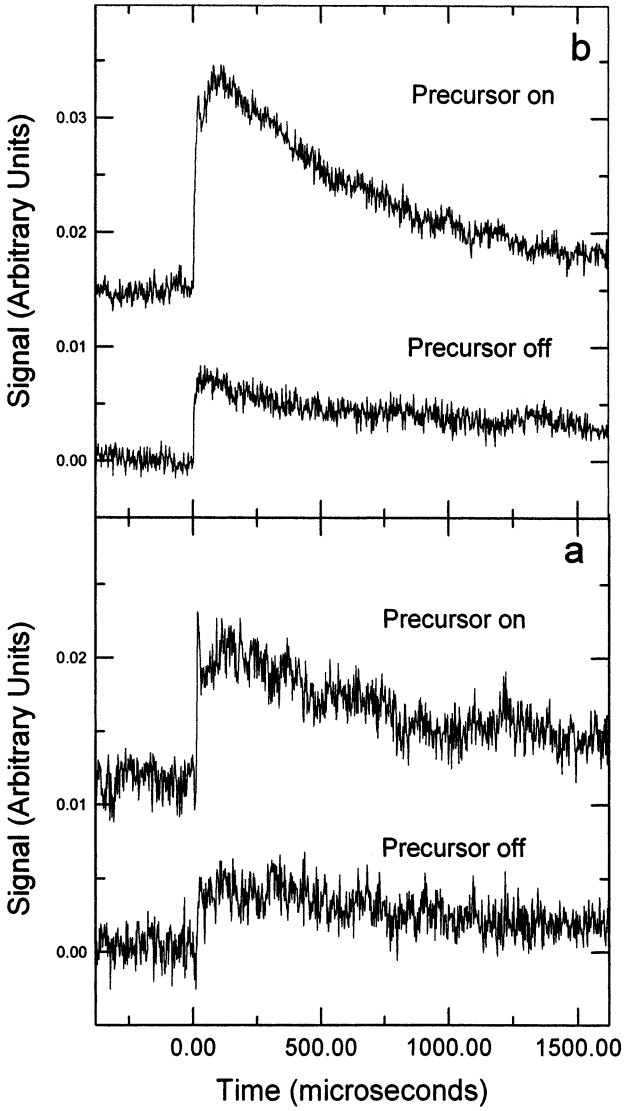

Figure 6. Transient signals of (a) H_2CO and (b) NO. Reaction conditions: $P(H_2O_2) = 0.50$ Torr (upper traces), $P(H_2O_2) = 0.0$ Torr (lower traces), $P(HCNO) = 0.20$ Torr, and $P(SF_6) = 1.00$ Torr.

Transient signal amplitudes (peak−peak) were converted into absolute concentration using HITRAN linestrengths for CO, CO_2, N_2O, CH_2O, and NO, as described in previous publications.[26] For HNO, no literature linestrengths were available. As a result, absolute calibration of HNO signals was done as follows: HNO and CO transient signals from 248 nm photolysis of an ICN/H_2CO/NO/buffer gas mixture were observed. These signals are attributed to the following reaction sequence

$$ICN + h\nu\ (248\ nm) \rightarrow I + CN \quad (8)$$

$$CN + H_2CO \rightarrow HCN + HCO \quad (9)$$

$$HCO + NO \rightarrow HNO + CO \quad (10)$$

Reactions 9 and 10 are fast, with $k_9 = 1.7 \times 10^{-11}$ cm^3 molecule^{-1} s^{-1} at 300 K[33,34] and $k_{10} = 1.2 \times 10^{-11}$ cm^3 molecule^{-1} s^{-1} at 296 K.[35] Provided that an excess of H_2CO and NO are present, we expect quantitative conversion of CN radicals into HNO + CO products. The HNO concentration may therefore be assumed to be equal to the CO concentration, which was obtained from HITRAN linestrengths. In addition, the HNO (and CO) concentrations should be approximately equal to the initial number of CN radicals present, which was estimated from

TABLE 1: Product Yields of Reaction OH + HCNO

product	without H_2O_2[a]	with H_2O_2[a]	difference[a,b]	excimer pulse energy (mJ)	relative yield[c]
NO	0.748	1.23	0.481	4.56	0.033
H_2CO	0.0	0.376	0.376	4.11	0.029
HNO	1.46	6.24	4.78	3.94	0.378
CO (without O_2)	6.20	16.83	10.63	3.80	0.872
CO (with O_2)	9.43	21.11	11.68	3.64	1.00
N_2O[d]	5.13	4.24	−0.891	5.52	

[a] In units of 10^{12} molecule cm^{-3}. [b] Obtained by subtracting yields in column 2 from yields in column 3. [c] Relative yields attributed to the title reaction, obtained from difference yields (column 4) after correction for excimer pulse energy (column 5) and normalized to [CO] = 1.00 [d] N_2O yields obtained in the presence of NO.

the photolysis laser energy, the 248 nm absorption coefficient of the ICN precursor ($\alpha = 0.009$ cm^{-1} $Torr^{-1}$),[26] and an assumed photolysis quantum yield of unity. These two calibrations gave the same result to within ~15% uncertainty. The comparison of the HNO concentration to the HNO transient signal therefore provided the calibration, which was applied to the HNO transient signals observed in the title reaction.

Table 1 shows a typical dataset of product molecule yields. Shown are concentrations obtained both with and without the H_2O_2 precursor and the difference between these two measurements. In addition, a small correction was made to account for variations in excimer laser pulse energies over the course of the experiment. The right-hand column of Table 1 shows the resulting relative product yields.

These product yield measurements suffer from one major background source, which is the direct photolysis of the HCNO reactants. No detailed study of HCNO photophysics has been reported, but a UV−vis spectrum of our HCNO samples shows strong absorption at 193 nm and weaker but still significant absorption at 248 nm. (It is for this reason that we chose to use the H_2O_2 precursor, reaction 6, rather than reactions 4 and 5 for the product yield measurements.) We believe that HCNO photolysis is probable and is responsible for the observations of product yields even in the absence of our OH precursor. Several photolysis products are energetically possible at a 248 nm photolysis wavelength

$$\mathrm{HCNO} + h\nu\ (248\ \mathrm{nm}) \rightarrow \mathrm{H} + (\mathrm{NCO}) \quad (11a)$$

$$\rightarrow (\mathrm{HCN}) + \mathrm{O} \quad (11b)$$

$$\rightarrow \mathrm{NH} + \mathrm{CO} \quad (11c)$$

No information on the relative quantum efficiencies of these products is available, but it is apparent that the products observed upon photolysis of a $HCNO/SF_6$ mixture may be formed either directly by photolysis or by further chemistry of radicals formed in reaction 11 with other species (including HCNO itself). For example, we can speculate that perhaps (some) of the following reactions occur

H + HCNO

$$\rightarrow \mathrm{CH_2} + \mathrm{NO} \quad \Delta H^0_{298} = -87.4\ \mathrm{kJ/mol} \quad (12a)$$

$$\rightarrow \mathrm{CO} + \mathrm{NH_2} \quad \Delta H^0_{298} = -309.4\ \mathrm{kJ/mol} \quad (12b)$$

$$\rightarrow \mathrm{CH_2O} + \mathrm{N} \quad \Delta H^0_{298} = -32.5\ \mathrm{kJ/mol} \quad (12c)$$

NH + HCNO

$$\rightarrow \mathrm{CH_2O} + \mathrm{N_2} \quad \Delta H^0_{298} = -663.7\ \mathrm{kJ/mol} \quad (13a)$$

$$\rightarrow \mathrm{NH_2} + (\mathrm{NCO}) \quad \Delta H^0_{298} = -225.6\ \mathrm{kJ/mol} \quad (13b)$$

$$\rightarrow \mathrm{HCN} + \mathrm{HNO} \quad \Delta H^0_{298} = -313.1\ \mathrm{kJ/mol} \quad (13c)$$

O + HCNO

$$\rightarrow \mathrm{OH} + (\mathrm{NCO}) \quad \Delta H^0_{298} = -250.0\ \mathrm{kJ/mol} \quad (14a)$$

$$\rightarrow \mathrm{CO} + \mathrm{HNO} \quad \Delta H^0_{298} = -431.4\ \mathrm{kJ/mol} \quad (14b)$$

$$\rightarrow \mathrm{HCO} + \mathrm{NO} \quad \Delta H^0_{298} = -286.6\ \mathrm{kJ/mol} \quad (14c)$$

The product list in the above reactions is not exhaustive, and this chemistry at the present time remains almost completely unexplored, making any detailed modeling of our reaction system impractical. As an approximate procedure, we have therefore chosen to simply subtract the product yields obtained in the absence of H_2O_2 precursor from the yields obtained with precursor present to estimate the product yields produced in the title reaction. This approach is not completely satisfactory, as H_2O_2 may somewhat affect the secondary chemistry of some of the radicals formed in reaction 11. Nevertheless, this procedure at least allows us to make semiquantitative conclusions regarding the major product channels of the title reaction.

Table 1 shows that the N_2O yield upon photolysis of an $HCNO/NO/SF_6$ mixture is actually somewhat greater than the yield upon photolysis of an $H_2O_2/HCNO/NO/SF_6$ mixture. We attribute the N_2O yield obtained from the $HCNO/NO/SF_6$ mixture to the formation of NCO (or possibly CNO) by direct photolysis, reaction 11a, followed by reaction 7. It is also possible that some of this N_2O originates from photolysis channel 11c followed by NH + NO secondary chemistry. The decreased yield obtained when the H_2O_2 precursor is included may be due to a reaction of NCO with H_2O_2, which would compete with reaction 7, although no literature data exists on this reaction. In any case, since the N_2O yield did not increase upon including H_2O_2 in the reaction, we conclude that channel 3a in the title reaction is minor or insignificant. If we assume that at least a 10% increase in the N_2O yield (comparing with and without H_2O_2) is the minimum detectable, then we estimate an upper limit for the branching ratio in channel 3a to be $\varphi_{3a} < 0.05$.

For the other detected products, significant amounts were detected in the absence of H_2O_2, but the yields were observed to increase substantially when H_2O_2 was included. For the CO, H_2CO, and HNO products, we estimated the contribution of the title reaction by subtracting the product yield obtained upon photolysis of HCNO/buffer gas from that obtained upon photolysis of H_2O_2/HCNO/buffer gas mixtures. Table 1 shows the results for a typical experimental run.

Examination of Table 1 shows that the yields of NO and H_2CO are approximately the same. This strongly suggests that both of these products originate predominately from channel 3e and that channel 3g, which would form an excess of NO, is comparatively insignificant. The yields of NO and H_2CO are, however, much less than the yields of HNO and CO. This suggests that channel 3e is in fact a rather minor channel and that either 3c or 3f dominate the reaction.

Channel 3c could be a source of CO products, because secondary reactions of HCO could easily form CO. For example, if trace amounts of oxygen are present

$$\mathrm{HCO} + \mathrm{O_2} \rightarrow \mathrm{CO} + \mathrm{HO_2} \quad (15)$$

TABLE 2: Product Branching Ratios of the OH + HCNO Reaction[a]

product channel	branching fraction
$CO + H_2NO$ (3f)	0.61 ± 0.06
$HNO + HCO$ (3c)	0.35 ± 0.06
$NO + H_2CO$ (3e)	0.04 ± 0.02

[a] Assumes no other product channels are active.

could occur. Other HCO secondary chemistry may be possible as well, along with simple HCO → H + CO dissociation. In some experiments, we included O_2 as a reagent in the reaction mixture, to convert any HCO formed into CO via reaction 15. As shown in Table 1, this resulted in a moderate increase in the observed CO yield. This result certainly suggests that at least some of the observed CO originates from HCO, however, the CO yield is much in excess of the HNO yield, so channel 3c cannot account for all of the observed CO. We believe that the CO yield obtained in the presence of excess O_2 is in fact measuring the contribution of CO from channel 3f as well as the HCO from 3c. We estimate the contribution of 3f by subtracting the HNO yield from the CO yield (with O_2 included) and conclude that 3f is in fact the major channel of the title reaction. Table 2 shows the estimated branching ratios obtained, where we have assumed that 3c, 3e, and 3f are the only active product channels (i.e., the totals are normalized to unity). The total yield of 3c + 3e + 3f is consistent with an order of magnitude estimate of $[OH]_0 \sim 10^{13}$ molecules cm^{-3}, but we cannot exclude the possibility that other product channels may exist as well. Although different data sets give very consistent results to within approximately 2%, the error bars in Table 2 are somewhat greater to account for possible systematic errors, considering the potential secondary chemistry described above.

4. Discussion

Our results represent the first experimental study of the title reaction. The only literature comparison is an estimated total rate constant for modeling purposes and a computational study of the OH + HCNO potential energy surface at the HL1 level of theory.[1] Our total rate constant at 296 K is nearly exactly the value of 3.32×10^{-11} cm^3 $molecule^{-1}$ s^{-1} used in the modeling study. That study, however, made no estimate of temperature dependence. An extrapolation of our measurements to the temperature range $T = 1200-1500$ K relevant in NO-reburning suggests a rate constant nearly an order of magnitude below our 296 K value, although clearly such an extrapolation is not warranted by the narrow temperature range of our data.

Several experimental artifacts can cause systematic errors in a pseudo-first-order kinetics experiment. The first, decomposition of HCNO samples during the experiments, was minimized by completing a single OH LIF decay measurement in about 4 min (typically, this allows 3 min for filling the cell and allowing the reagents to mix and 1 min for the LIF data collection). In this amount of time, less than 10% decomposition occurs, as shown in Figure 1. A related issue is the possible reaction of OH radicals with decomposition products, photoproducts, or reaction products from the title and/or secondary reactions. By using an estimated absorption cross section of HCNO at 248 nm of 1.41×10^{-19} cm^2, and assuming a photolysis quantum yield of unity, we estimate $\sim 6 \times 10^{12}$ cm^{-3} of HCNO photolysis products from a 5 mJ excimer pulse at $P_{HCNO} = 0.06$ Torr (the highest pressure used in Figure 3). This is comparable to our estimated values of $[OH]_0$, but represents only approximately 0.3% conversion of the initial HCNO. Because our measured rate constants are within an order of magnitude of the gas kinetic, the reaction of OH with transient species produced by HCNO photolysis is clearly not a severe problem. If k_3 were several orders of magnitude slower, such secondary chemistry would be a much more serious problem. A more problematic issue is the reaction of OH with stable products, which could potentially build up over the ~50 laser shots required to obtain one of the data sets of Figure 2. A simple test for this effect is to simply measure the OH decay twice in rapid succession on the same gas fill. If the OH reaction with stable products were a significant problem, we would expect the second measurement to yield a higher value of the pseudo-first-order OH decay rate. In fact, we observe only a slight decrease in this decay rate on the second measurement, consistent with a slight decomposition of HCNO over time.

The mechanism of this reaction likely proceeds from OH attack at the carbon of HCNO to form a HC(OH)NO complex. Hydrogen atom migration via a four-center transition state can form a HC(O)N(H)O complex, which may then dissociate by C−N bond fission to form HCO + HNO, channel 3c. Alternatively, this complex may undergo a second hydrogen atom migration via a three-center transition state to form an $OCNH_2O$ complex, which may dissociate to $CO + H_2NO$ products, channel 3f. The first of these possibilities, channel 3c, was predicted in the potential energy surface of Miller et al.[1] That study did not consider the possibility of channel 3f, however. That study also predicted a low-energy pathway to $H_2 + CO + NO$ products, channel 3g. Our observation of very low NO yields suggests that this is not a major channel. Pathways to channel 3a involve two hydrogen migrations to the terminal oxygen of HCNO. The second of these migrations involves a moderately higher barrier, but the authors still predicted a moderate yield of NCO-forming channels.[1] Our experiments indicate that formation of NCO is at most a very minor pathway in this reaction. Pathways to other product channels, such as 3d, were predicted to have high energy barriers.

5. Conclusion

The kinetics and product branching of the OH + HCNO reaction were studied using laser-induced fluorescence and IR diode laser absorption spectroscopy. The reaction is fast, with $k = (3.39 \pm 0.3) \times 10^{-11}$ cm^3 $molecule^{-1}$ s^{-1} at 296 K, and has a moderate, negative temperature dependence. The major product channels are $CO + H_2NO$ and HCO + HNO.

Acknowledgment. This work was supported by the Division of Chemical Sciences, Office of Basic Energy Sciences of the Department of Energy, Grant DE-FG03-96ER14645.

References and Notes

(1) Miller, J. A.; Klippenstein, S. J.; Glarborg, P. *Combust. Flame* **2003**, *135*, 357.
(2) Boullart, W.; Ngugen, M. T.; Peeters, J. *J. Phys. Chem*. **1994**, *98*, 8036.
(3) Eickhoff, U.; Temps, F. *Phys. Chem. Chem. Phys*. **1999**, *1*, 243.
(4) Vereecken, L.; Sumathy, R.; Carl, S. A.; Peeters, J. *Chem. Phys. Lett*. **2001**, *344*, 400.
(5) Tokmakov, I. V.; Moskaleva, L. V.; Paschenko, D. V.; Lin, M. C. *J. Phys. Chem. A* **2003**, *107*, 1066.
(6) Meyer, J. P.; Hershberger, J. F. *J. Phys. Chem. B* **2005**, *109*, 8363.
(7) Chase, M. W., Jr. *NIST-JANAF Thermochemical Tables*, 4th ed; Journal of Physical and Chemical Reference Data; American Chemical Society: Washington , DC, 1998.
(8) East, A. L. L.; Allen, W. D. *J. Chem. Phys*. **1993**, *99*, 4638.
(9) Sumathi, R.; Sengupta, D.; Nguyen, M. T. *J. Phys. Chem. A* **1998**, *102*, 3175.
(10) Tsang, W. *J. Phys. Chem. Ref. Data* **1992**, *21*, 753.
(11) Miller, J. A.; Melius, C. F. *Int. J. Chem. Kinet.* **1992**, *24*, 421.

(12) Mertens, J. D.; Hanson, R. K. *Symp. (Int). Combust. [Proc.]* **1996**, *26*, 551.
(13) Nguyen, M. T.; Sengupta, D.; Vereecken, L.; Peeters, J. Vanquickenborne, L. G. *J. Phys. Chem.* **1996**, *100*, 1615.
(14) Mertens, J. D.; Kohse-Hoinghaus, K.; Hanson, R. K. Bowman, C. T. *Int. J. Chem. Kinet.* **1991**, *23*, 655.
(15) Wooldridge, M. S.; Hanson, R. K.; Bowman, C. T. *Int. J. Chem. Kinet.* **1996**, *28*, 361.
(16) Mertens, J. D.; Change, A. Y.; Hanson, R. K.; Bowman, C. T. *Int. J. Chem. Kinet.* **1992**, *24*, 2479.
(17) Tully, F. P.; Perry, R. A.; Thorne, L. R.; Allendorf, M. D. *Symp. (Int.) Combust. [Proc.]* **1989**, *22*, 1101.
(18) Ongstad, A. P.; Liu, X.; Coombe, R. D. *J. Phys. Chem.* **1988**, *92*, 5578.
(19) Liu, X.; Machara, N. P.; Coombe, R. D. *J. Phys. Chem*. **1991**, 95, 4983.
(20) Pasinszki, T.; Kishimoto, N.; Ohno, K. *J. Phys. Chem*. **1999**, *103*, 6746.
(21) Wentrup, C.; Gerecht, B.; Briehl, H. *Angew. Chem., Int. Ed. Engl.* **1979**, *18*, 467.
(22) Wilmes, R.; Winnewisser, M. *J. Labelled Compd. Radiopharm*. **1993**, *33*, 157.
(23) Rothman, L. S.; et al. *J. Quant. Spectrosc. Radiat. Transfer* **1992**, *48*, 469.
(24) Ferretti, E. L.; Rao, K. N. *J. Mol. Spectrosc*. **1974**, *51*, 97.
(25) Johns, J. W. C.; McKellar, A. R. W.; Weinberger, E. *Can. J. Phys*. **1983**, *61*, 1106.
(26) Cooper, W. F.; Park, J.; Hershberger, J. F. *J. Phys. Chem*. **1993**, *97*, 3283.
(27) Cooper, W. F.; Hershberger, J. F. *J. Phys. Chem*. **1992**, *96*, 771.
(28) Meyer, J. P.; Hershberger, J. F. *J. Phys. Chem. A* **2005**, *109*, 4772.
(29) Fakhr, A.; Bates, R. D., Jr. *Chem. Phys. Lett*. **1980**, *71*, 381.
(30) Stephenson, J. C.; Moore, C. B. *J. Chem. Phys*. **1970**, *52*, 2333.
(31) Richman, D. C.; Millikan, R. C. *J. Chem. Phys*. **1975**, *63*, 2242.
(32) Green, W. H.; Hancock, J. K. *J. Chem. Phys*. **1973**, *59*, 4326.
(33) Yu, T.; Yang, D. L.; Lin, M. C. *Int. J. Chem. Kinet*. **1993**, *25*, 1053.
(34) Chang, Y.-W.; Wang, N. S. *Chem. Phys*. **1995**, *200*, 431.
(35) Tsang, W.; Herron, J. T. *J. Phys. Chem. Ref. Data* **1991**, *20*, 609.